Static Analysis of Microstrip Discontinuities Using the Excess Charge Density in the Spectral Domain

Jesús Martel, Rafael R. Boix, and Manuel Horno, *Member, IEEE*

Abstract—**Galerkin's method in the spectral domain is applied to solve for the excess charge density existing on the strips of open-end and symmetric gap discontinuities in multilayered anisotropic substrates. The excess charge density is used to determine the capacitance components of the equivalent circuits of these discontinuities. Numerical results are provided and a comparison with previous results existing in the literature is carried out.**

I. Introduction

MICROSTRIP circuits are invariably accompanied by discontinuities. The rigorous characterization of these discontinuities requires a determination of their frequency-dependent scattering parameters by means of a full-wave analysis [1], [2]. However, at low frequencies, microstrip discontinuities can be characterized by equivalent circuits consisting of lumped capacitances and inductances [3], [4].

The aim of this work is the calculation of the lumped capacitances of the equivalent circuits that are employed to characterize the open-end microstrip discontinuity and the symmetric gap microstrip discontinuity. In the literature, two different techniques have been used to calculate these lumped capacitances. The first technique involves the calculation of the capacitance parameters of single and coupled rectangular microstrip patches [4]–[8], and it has the inherent disadvantage of involving the subtraction of two similar quantities that have to be numerically computed [9]. The second technique is based on the calculation of the excess charge density existing on the strips of the discontinuity with respect to that existing on the strip of an infinite microstrip line [9]–[11]. This technique avoids the errors arising from the subtraction of two close quantities that have to be numerically computed, and it is the technique employed here.

Whereas in previous works the excess charge technique was applied in the spatial domain [9]–[11], in this paper the excess charge density technique is applied in the spectral domain. This makes it possible to analyze microstrip discontinuities embedded in multilayered media with dielectric anisotropy in an easy way [8].

Manuscript received December 4, 1990; revised April 22, 1991. This work was supported by the DGICYT, Spain (Proj. n. PB87-0798-CO3-01).

The authors are with the Department of Electronics and Electromagnetism, University of Seville, Avd. Reina Mercedes s/n, 41012 Seville, Spain.

IEEE Log Number 9101656.

The results obtained for the lumped capacitances of the two discontinuities analyzed have been compared with results obtained by means of static analyses [6]–[9] and with results extrapolated from dynamic analyses [2]. Discrepancies are encountered, which are attributed to the lack of accuracy of existing results.

II. Analysis

In Fig. 1(a) is shown the cross section of both the microstrip open-end discontinuity appearing in Fig. 1(b) and the microstrip gap discontinuity appearing in Fig. 1(c). The conducting strips of the open-end discontinuity and the gap discontinuity are assumed to be lossless and infinitely thin. These conducting strips are placed at the Mth interface of a stratified medium bounded by two grounded conducting planes. The stratified medium is composed of N layers of lossless anisotropic dielectric materials. The dielectric materials are assumed to present uniaxial anisotropy, their optical axes being aligned with the y axis defined in parts (a)–(c) of Fig. 1. According to this, each dielectric material in the stratified medium is characterized by a permittivity tensor:

$$\hat{\epsilon}^i = \epsilon_0 \begin{pmatrix} \epsilon_{11}^i & 0 & 0 \\ 0 & \epsilon_{22}^i & 0 \\ 0 & 0 & \epsilon_{11}^i \end{pmatrix} \qquad (1)$$

$$(i = 1, \cdots, N).$$

At low frequencies, the microstrip discontinuities shown in parts (b) and (c) of Fig. 1 can be characterized by the lumped element equivalent circuits shown in, respectively, parts (d) and (e). In the following, we will explain how to calculate the lumped capacitances C_{oc}, C_{pg}, and C_{sg}.

A. Calculation of C_{oc}

The free superficial charge density $\sigma(x, z)$ on the semi-infinite strip of the open-end discontinuity shown in Fig. 1(b) can be separated into two terms:

$$\sigma(x, z) = \sigma_\infty(x)u(z) + \sigma_{ex}(x, z). \qquad (2)$$

The first term can be interpreted as the charge density that would exist on half the strip of the microstrip line

0018-9480/91/0900-1623$01.00 ©1991 IEEE

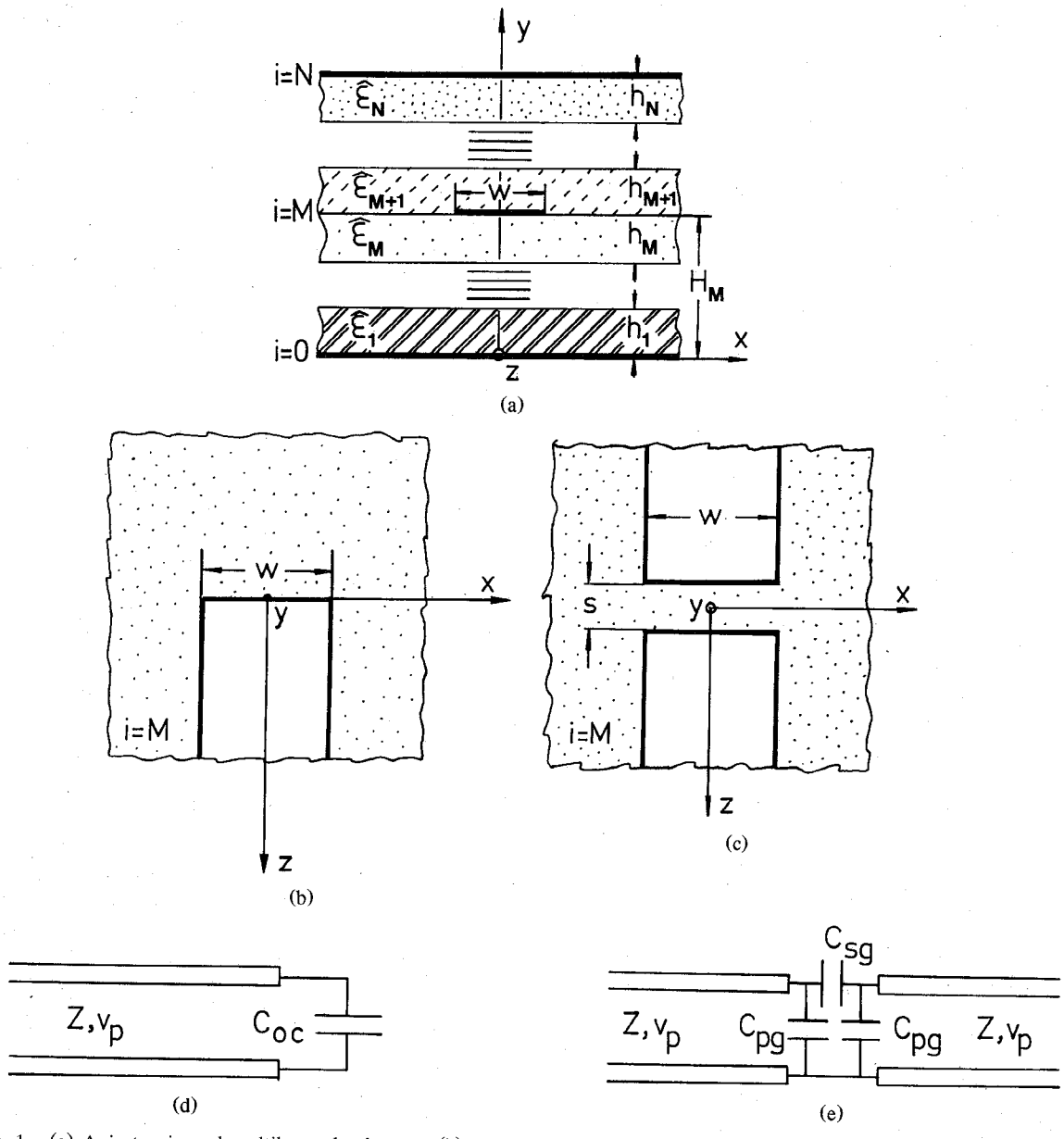

Fig. 1. (a) Anisotropic and multilayered substrate. (b) Strip of an open-end microstrip discontinuity lying on the Mth interface of the multilayered substrate shown in (a). (c) Strips of a symmetric gap microstrip discontinuity lying on the Mth interface of the multilayered substrate shown in (a). (d) Equivalent circuit of the open-end discontinuity. (e) Equivalent circuit of the symmetric gap discontinuity.

involved in the discontinuity if this microstrip line were infinite. This term is the product of the free superficial charge density per unit length existing on the strip of the infinite microstrip line $\sigma_\infty(x)$ and the step function $u(z)$. The second term, $\sigma_{ex}(x,z)$, represents the excess free superficial charge density which is stored in the neighborhood of the strip end at the open-end discontinuity. The edge capacitance of the open-end microstrip can be calculated from this excess charge density by means of the expression

$$C_{oc} = \frac{\int_0^\infty \int_{-w/2}^{+w/2} \sigma_{ex}(x,z)\,dx\,dz}{V} \tag{3}$$

where V is the known constant potential on the semi-infinite strip. As can be seen from (3), in order to calculate C_{oc}, it suffices to determine the excess charge density, $\sigma_{ex}(x,z)$. In this paper, we have focused our attention on calculating the two-dimensional Fourier transform of the excess charge density, namely, $\tilde{\sigma}_{ex}(\alpha,\beta)$. In terms of $\tilde{\sigma}_{ex}(\alpha,\beta)$, C_{oc} can be simply obtained.

To obtain $\tilde{\sigma}_{ex}(\alpha,\beta)$, we have made use of the expression that relates the excess charge density, $\sigma_{ex}(x,z)$, and the electrostatic potential, $\phi(x, y = H_M, z)$, at the Mth interface of Fig. 1(b), i.e.

$$\begin{aligned}\phi(x, y = H_M, z) &= \int_{-\infty}^{+\infty}\int_{-\infty}^{+\infty} G(x-x', y = H_M, y' = H_M, z-z') \\ &\quad \cdot \left[\sigma_\infty(x')u(z') + \sigma_{ex}(x',z')\right] dx'\,dz'\end{aligned} \tag{4}$$

where $G(x-x', y=H_M, y'=H_M, z-z')$ is the dielectric Green's function of the problem when the field point and the source point lie on the mth interface. If we apply two-dimensional Fourier transforms to (4), the following algebraic relation in the spectral domain is obtained:

$$\tilde{\phi}(\alpha, y=H_M, \beta) = \tilde{G}(\alpha,\beta)\left[\tilde{\sigma}_\infty(\alpha)\tilde{u}(\beta) + \tilde{\sigma}_{ex}(\alpha,\beta)\right]. \tag{5}$$

The spectral Green's function, $\tilde{G}(\alpha,\beta)$, appearing in this expression can be analytically obtained by using the recurrent algorithm developed in [8]. The Fourier transform of the free superficial charge density per unit length, $\tilde{\sigma}_\infty(\alpha)$, can also be calculated by applying the Galerkin method in the spectral domain, as shown elsewhere [12]. In fact, when the Galerkin method is used, the spatial charge density per unit length, $\sigma_\infty(x)$, is obtained as a weighted basis functions expansion of the following type:

$$\sigma_\infty(x) = \sum_{n=0}^{N_1} a_n \sigma_\infty^n(x). \tag{6}$$

Assuming $\tilde{G}(\alpha,\beta)$ and $\tilde{\sigma}_\infty(\alpha)$ are known functions, the Galerkin method in the spectral domain has been employed in (5) to calculate $\tilde{\sigma}_{ex}(\alpha,\beta)$. For that purpose, the excess charge density, $\sigma_{ex}(x,z)$, has been expanded in terms of basis functions as indicated below:

$$\sigma_{ex}(x,z) = \sum_{n=0}^{N_1}\sum_{m=0}^{N_2} b_{nm}\sigma_\infty^n(x)\sigma^m(z). \tag{7}$$

As can be seen, the basis functions in (7) have been factored into two independent functions of the spatial variables x and z. The functions $\sigma_\infty^n(x)$ coincide with those used in (6). This means that we have assumed that the charge density per unit length on the strip of the infinite microstrip line, $\sigma_\infty(x)$, and the excess charge density, $\sigma_{ex}(x,z)$, depend on the x variable in the same way. This assumption simplifies the mathematical treatment of the problem and it only seems to be far from reality (see Fig. 1(b)) in the neighborhood of the 90° conductor corners where the singular behavior of $\sigma_{ex}(x,z)$ differs from that of $\sigma_\infty(x)$ [13]. When the two-dimensional Fourier transforms of expressions (6) and (7) are introduced into (5) and Galerkin method in the spectral domain is used, the following system of linear equations for the b_{nm} coefficients is obtained:

$$2\pi^2 V\tilde{\sigma}_\infty^k(\alpha=0)\tilde{\sigma}^l(\beta=0) - \sum_{n=0}^{N_1} a_n \Lambda_{nk}^l = \sum_{n=0}^{N_1}\sum_{m=0}^{N_2} b_{nm}\Gamma_{nk}^{ml} \tag{8}$$

$$(k=0,\cdots,N_1;\ l=0,\cdots,N_2)$$

where Λ_{nk}^l and Γ_{nk}^{ml} are double integrals with infinite limits that can be expressed as

$$\Lambda_{nk}^l = \int_{-\infty}^{+\infty}\int_{-\infty}^{+\infty} \tilde{G}(\alpha,\beta)\tilde{\sigma}_\infty^n(\alpha)\frac{1}{j\beta}\tilde{\sigma}_\infty^{k*}(\alpha)\tilde{\sigma}^{l*}(\beta)\,d\alpha\,d\beta \tag{9}$$

$$(n,k=0,\cdots,N_1;\ l=0,\cdots,N_2)$$

$$\Gamma_{nk}^{ml} = \int_{-\infty}^{+\infty}\int_{-\infty}^{+\infty} \tilde{G}(\alpha,\beta)\tilde{\sigma}_\infty^n(\alpha)\cdot\tilde{\sigma}^m(\beta)\tilde{\sigma}_\infty^{k*}(\alpha)\tilde{\sigma}^{l*}(\beta)\,d\alpha\,d\beta \tag{10}$$

$$(n,k=0,\cdots,N_1;\ m,l=0,\cdots,N_2).$$

In this work, to represent the functions $\sigma_\infty^n(x)$ and $\sigma^m(z)$ defined in (6) and (7), we have chosen the functions

$$\sigma_\infty^n(x) = \frac{2}{\pi w}\frac{T_{2n}\left(\dfrac{2x}{w}\right)}{\left[1-\left(\dfrac{2x}{w}\right)^2\right]^{1/2}} \tag{11}$$

$$(n=0,\cdots,N_1)$$

$$\sigma^m(z) = \frac{1}{z_{m+1}-z_m}\left[u(z-z_{m+1}) - u(z-z_m)\right] \tag{12}$$

$$(m=0,\cdots,N_2)$$

$$z_0=0;\ z_0<z_1<\cdots<z_{N_2+1}$$

or

$$\sigma^0(z) = \begin{cases} \dfrac{2(z_1-z)}{(z_1-z_0)^2}, & z_0 \le z < z_1 \\ 0, & \text{elsewhere} \end{cases}$$

$$\sigma^m(z) = \begin{cases} \left(\dfrac{z-z_{m-1}}{z_m-z_{m-1}}\right)\left(\dfrac{2}{z_{m+1}-z_{m-1}}\right), & z_{m-1}\le z<z_m \\ \left(\dfrac{z_{m+1}-z}{z_{m+1}-z_m}\right)\left(\dfrac{2}{z_{m+1}-z_{m-1}}\right), & z_m \le z<z_{m+1} \\ 0, & \text{elsewhere} \end{cases} \tag{13}$$

$$(m=1,\cdots,N_2)$$

$$z_0=0;\ z_0<z_1<\cdots<z_{N_2+1}.$$

In (11), T_{2n} are even Chebyshev polynomials of the first kind. In choosing $\sigma_\infty^n(x)$ and $\sigma^m(z)$, we have tried to satisfy the known physical constraints of $\sigma_{ex}(x,z)$ as accurately as possible. For instance, the functions defined in (11) properly account for the singular behavior of $\sigma_{ex}(x,z)$ in $x=\pm w/2$ except in the neighborhood of the $z=0$ plane [13]. Concerning the functions defined in (12) (pulse functions, Fig. 2(a)) and in (13) (triangle functions, Fig. 2(b)), these functions do not seem to account for the singularity that $\sigma_{ex}(x,z)$ presents at the $z=0$ plane of Fig. 1(b). In any event, this singularity has been simulated in an approximated way by choosing nonequispaced grid points in the piecewise approximation of the $\sigma_{ex}(x,z)$ dependence on the z variable. In order to choose the grid points z_m $(m=0,\cdots,N_2+1)$ defined in (12) and (13), we have made use of the technique employed in [14] to

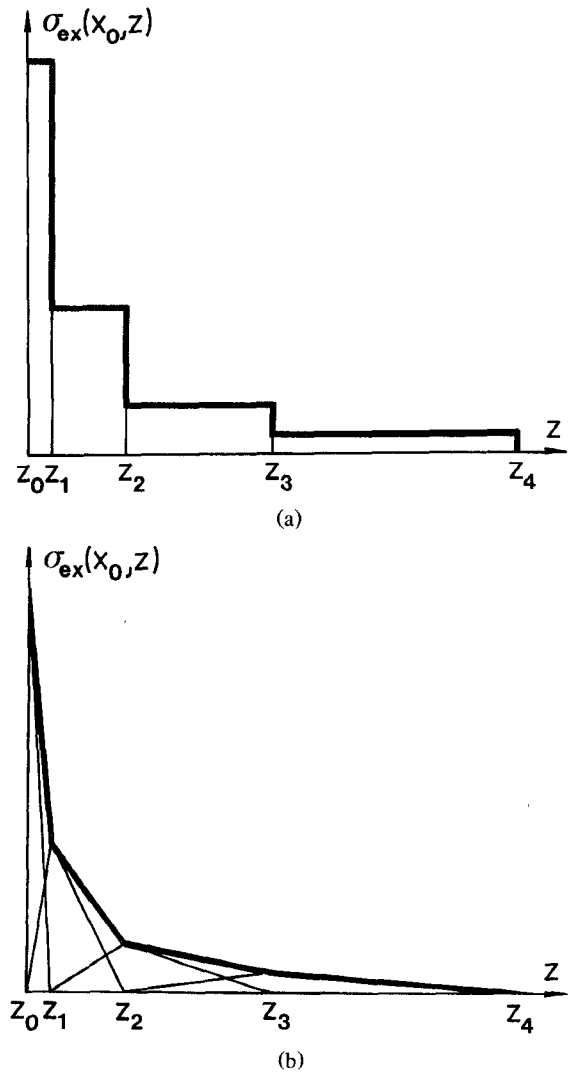

Fig. 2. Piecewise approximation of the $\sigma_{ex}(x,z)$ dependence on z using (a) pulse functions ($N_2 = 3$) and (b) triangle functions ($N_2 = 3$).

approximate the charge density per unit length on an infinite conducting strip. To start with, we have assumed that the dependence of $\sigma_{ex}(x,z)$ on the z variable for a fixed value of the x variable ($x = x_0$) can be approximated as

$$\sigma_{ex}(x_0,z) = \begin{cases} \dfrac{1}{\sqrt{z}} + k_1 z + k_2, & 0 \leq z \leq a \\ 0, & z > a \end{cases} \tag{14}$$

where $a = z_{N_2+1}$ is the distance from the end of the strip ($z = 0$ plane in Fig. 1(b)) to the z plane in which $\sigma_{ex}(x,z)$ can be neglected (the optimal value of a has been calculated by means of a convergence analysis, which is presented in the next section) and the constants k_1 and k_2 are calculated by requiring that $\sigma_{ex}(x_0,a) = 0$ and $\dfrac{\partial}{\partial z}\sigma_{ex}(x_0,z)|_{z=a} = 0$. After determining the quantities a, k_1, and k_2, the grid points z_m defined in (12) and (13) have been estimated by requiring that the same amount of charge be located between any two consecutive points for the fixed value x_0 [14]. This condition can be mathematically expressed as

$$\frac{\displaystyle\int_{z_m}^{z_{m+1}} \left(\frac{1}{\sqrt{z}} + k_1 z + k_2\right) dz}{\displaystyle\int_0^a \left(\frac{1}{\sqrt{z}} + k_1 z + k_2\right) dz} = \frac{1}{N_2+1}. \tag{15}$$

It can be noticed that the function proposed in (14) to simulate the dependence of $\sigma_{ex}(x,z)$ on the z variable accounts for the $z^{-1/2}$ singularity that $\sigma_{ex}(x,z)$ exhibits at the points of the end of the strip which are not in the vicinity of the 90° corners. This ensures a nonoscillating piecewise approximation of the $\sigma_{ex}(x,z)$ dependence on the z variable near the singularity [14]. One point of numerical interest is the fact that the pulse functions in (12) and the triangle functions in (13) have been normalized to have unity area. Owing to the normalization, the coefficients b_{nm} must all have the same order of magnitude and this prevents the linear system in (8) from being ill conditioned [15].

The direct numerical computation of the double integrals obtained when the Fourier transforms of $\sigma_\infty^n(x)$ and $\sigma^m(z)$ (see (11), (12), and (13)) are introduced into (9) and (10) requires high CPU times. We have substantially reduced these CPU times by employing a method which is explained in detail in the Appendix.

B. Calculation of C_{pg} and C_{sg}

An excess charge scheme applied in the spectral domain has been also employed to determine the capacitances C_{sg} and C_{pg} of the π network used to characterize the symmetric gap discontinuity shown in Fig. 1(c). As in previous papers [10], we have calculated the excess charge density on the strips for two different modes of excitation: the even mode, in which both strips are raised at the same constant potential, and the odd mode, in which the strips are raised at opposite potentials. In the case of the even mode of excitation, we have calculated C_{oc}^e, which is the edge capacitance of an open-end microstrip line facing a magnetic wall. In the case of the odd mode of excitation, we have calculated C_{oc}^o, which is the edge capacitance of an open-end microstrip line facing an electric wall. These capacitances C_{oc}^e and C_{oc}^o are related to the capacitances C_{pg} and C_{sg} by means of the expressions [10]

$$C_{oc}^e = C_{pg} \tag{16}$$

$$C_{oc}^o = C_{pg} + 2C_{sg}. \tag{17}$$

As for the case of the open-end discontinuity, we have derived expressions which relate the two-dimensional Fourier transforms of the electrostatic potential at the Mth interface of Fig. 1(c) and the two-dimensional Fourier transforms of the excess charge density on the strips of the gap discontinuity (see (5)) in both the even mode and the odd mode. To solve for the two-dimensional Fourier transforms of the excess charge density in each mode, the Galerkin method in the spectral domain has been applied. The functions employed to approximate the depen-

TABLE I
CONVERGENCE ANALYSIS OF C_{oc}/w WITH THE NUMBER OF BASIS FUNCTIONS FOR AN OPEN-END DISCONTINUITY IN VACUUM ($w/h = 10$)

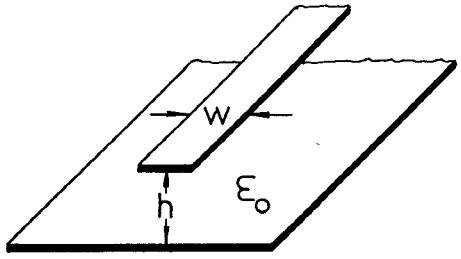

Number of basis functions		Pulse functions	Triangle functions
N_1+1	N_2+1	C_{oc}/w (pF/m)	C_{oc}/w (pF/m)
1	1	7.77	10.3
1	2	9.25	9.95
1	3	9.69	10.1
1	4	9.85	10.1
1	5	9.92	10.0
1	6	9.96	10.0
1	7	10.0	10.0
2	1	8.79	11.6
2	2	10.7	11.4
2	3	11.2	11.7
2	4	11.4	11.7
2	5	11.6	11.7
2	6	11.6	11.7
3	1	8.79	11.6
3	2	10.7	11.4
3	3	11.3	11.7
3	4	11.5	11.7
3	5	11.6	11.7
3	6	11.6	11.7

dence of the modal excess charge densities on the spatial variables x and z are analogous to those defined in (11), (12), and (13).

III. NUMERICAL CONVERGENCE

From a numerical point of view, the values of the capacitances C_{oc}, C_{sg}, and C_{pg} obtained by using the analysis method described in the preceding section depend mainly on three parameters:

- $N_1' = N_1 + 1$, the number of functions employed to approximate the excess charge density dependence on the x variable (see (11)).
- $N_2' = N_2 + 1$, the number of functions to approximate the excess charge density dependence on the z variable (see (12) and (13)).
- a, the distance from the end of the strips to the z plane in which the excess charge density is assumed to vanish.

In Table I, we provide the results obtained for the edge capacitance C_{oc} of an open-end discontinuity in vacuum when different values of N_1' and N_2' are used. Comparison is made between the results obtained by using pulse functions and triangle functions to approximate the $\sigma_{ex}(x, z)$ dependence on the z variable. It can be noticed that if triangle functions are used in the approximation of $\sigma_{ex}(x, z)$, the convergence to a fixed value of C_{oc} is achieved when $N_1' = 2$ and $N_2' = 3$. If pulse functions are used in the approximation of $\sigma_{ex}(x, z)$, we need to take at least $N_2' = 2$ and $N_2' = 6$ to achieve convergence. The convergence is faster in the case of triangle functions since these functions provide a continuous linear piecewise approximation of $\sigma_{ex}(x, z)$, which is better than the discontinuous step piecewise approximation provided by pulse functions. It has been observed that, for narrow strips ($w/h \leqslant 1$), it is only necessary to take $N_1' = 1$ to achieve convergence in the results of C_{oc} [16]. Similar results for the convergence of C_{sg} and C_{pg} with the number of basis functions have been found for the case of the symmetric gap.

TABLE II
CONVERGENCE ANALYSIS OF C_{oc}/w WITH THE DISTANCE a FOR AN OPEN-END DISCONTINUITY ($w/h = 1$). (a) IN VACUUM. (b) ON ALUMINA SUBSTRATE ($\epsilon_r = 9.6$)

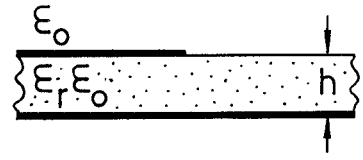

a/h	C_{oc}/w (pF/m)
6	13.5
8	13.7
10	13.8
12	13.9
14	13.9
16	14.0
18	14.0
20	14.0

(a)

a/h	C_{oc}/w (pF/m)
4	57.1
6	57.2
8	57.2
10	57.2
12	57.2

(b)

In Table II, we analyze how C_{oc} varies with increasing a in an open-end discontinuity in vacuum and an open-end discontinuity whose strip lies on alumina substrate. Whereas in the case of the open-end microstrip printed on alumina the excess charge is found to be concentrated within a length $a = 6h$, in the case of the open-end discontinuity in vacuum the excess charge density is found to be concentrated within a length $a = 16h$ at least.

In Table III, we analyze the variation of C_{oc}^e and C_{oc}^o in a symmetric gap discontinuity as the distance a increases. In strong coupling conditions ($s/w = 0.1$), the excess charge in the even mode is much more concentrated near the physical end of the discontinuity than the excess charge density in the odd mode. However, in weak coupling conditions ($s/w = 10$), the excess charge in both the even mode and the odd mode extends for similar lengths.

IV. RESULTS

In parts (a) and (b) of Fig. 3, we plot two sectional views of $\sigma_{ex}(x, z)$ for two different open-end microstrip discontinuities. It can be seen that as the permittivity of

TABLE III
CONVERGENCE ANALYSIS OF C^e_{oc} AND C^o_{oc} WITH THE DISTANCE a FOR A SYMMETRIC GAP DISCONTINUITY IN VACUUM ($w/h = 1$).
(a) STRONG COUPLING CONDITIONS ($s/w = 0.1$).
(b) WEAK COUPLING CONDITIONS ($s/w = 10$)

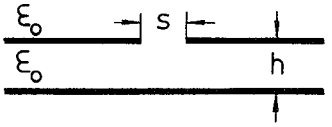

a/h	C^e_{oc}/w (pF/m)	C^o_{oc}/w (pF/m)
4	1.22	40.5
6	1.22	41.2
8	1.22	41.5
10	1.22	41.7
12	1.22	41.8
14	1.22	41.8

(a)

a/h	C^e_{oc}/w (pF/m)	C^o_{oc}/w(pF/m)
6	13.2	13.8
8	13.4	14.0
10	13.5	14.2
12	13.5	14.3
14	13.6	14.4
16	13.6	14.4

(b)

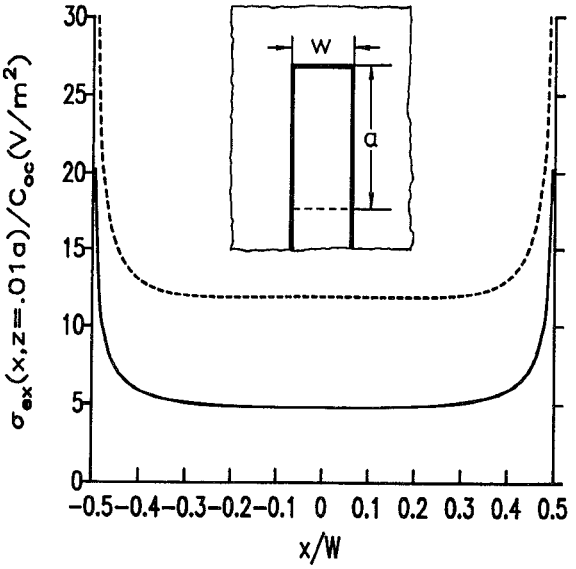

(a)

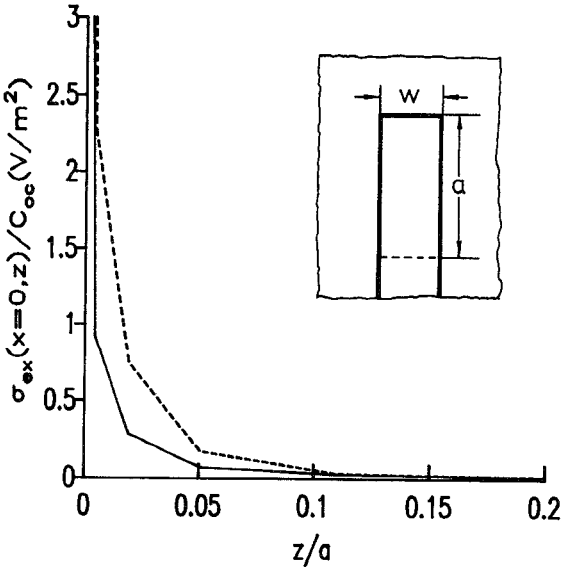

(b)

Fig. 3. Two sectional views of $\sigma_{ex}(x, z)/C_{oc}$. Solid lines stand for an open-end discontinuity in vacuum ($w/h = 1$; $a/h = 20$; $V = 1$ V), and dashed lines stand for an open-end discontinuity on alumina substrate ($\epsilon_r = 9.6$; $w/h = 1$; $a/h = 10$; $V = 1$ V).

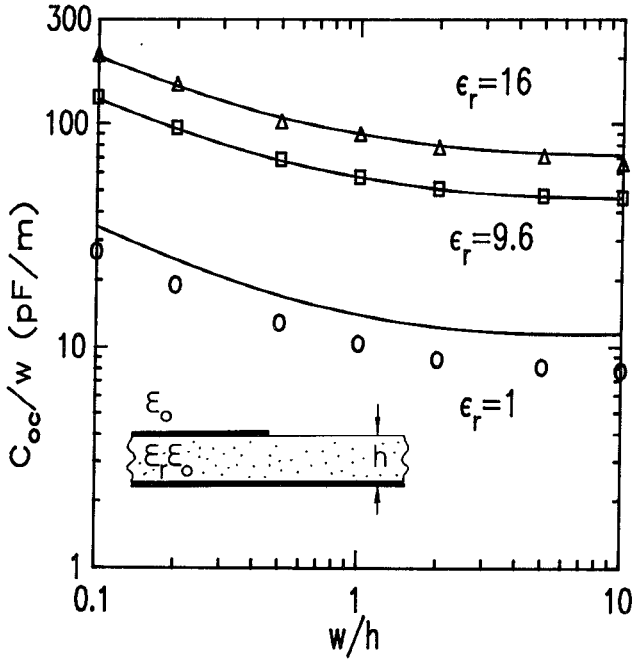

Fig. 4. Edge capacitance of open-end discontinuity (C_{oc}/w). Comparison with results reported in [6] (○), [9] (△) and [8] (□).

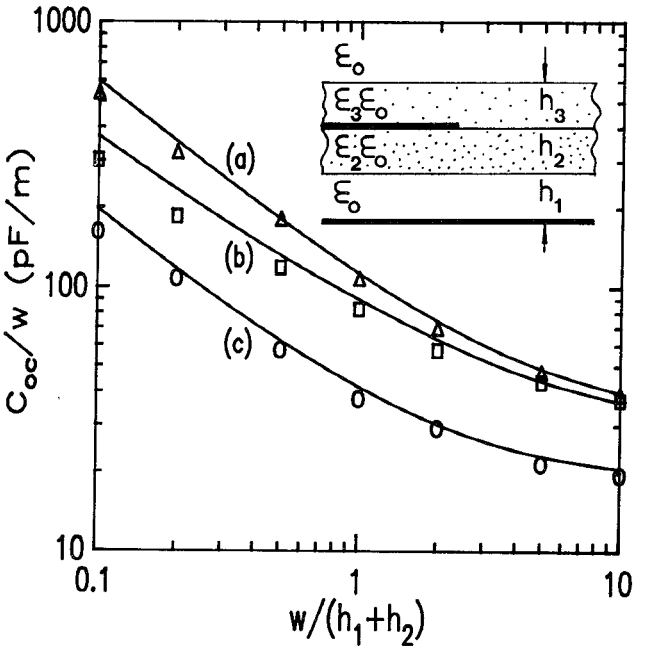

Fig. 5. Edge capacitance of open-end discontinuity (C_{oc}/w). (a) Sandwiched configuration ($h_2 = h_3 = 0.5h_1$, $\epsilon_2 = \epsilon_3 = 9.6$). (b) Inverted configuration ($h_1 = h_2 = 0.5h_3$, $\epsilon_2 = 1$, $\epsilon_3 = 9.6$). (c) Suspended configuration ($h_2 = 0.1h_1$, $\epsilon_3 = 1$, $\epsilon_2 = 9.6$). Comparison with the results appearing in [7] (△, □, ○).

the substrate increases, the excess charge becomes more concentrated around the physical end of the discontinuity.

In Fig. 4, the capacitance per unit strip width, C_{oc}/w, of several open-end microstrip discontinuities is plotted versus the ratio w/h. Comparison is made with the static results obtained by other authors using the rectangular patch technique [6], [8] and the excess charge technique [9]. Best agreement (within 2%) is found with the results

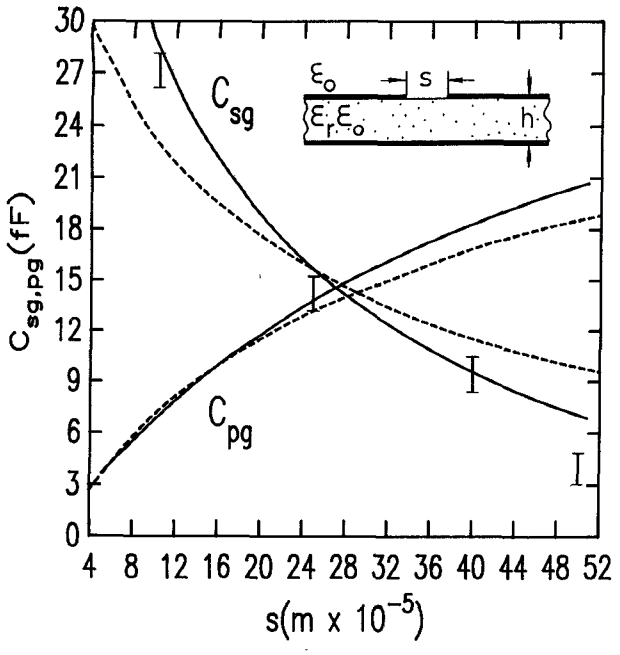

Fig. 6. Series and parallel capacitances of the equivalent circuit of a symmetric gap on a simple isotropic substrate ($\epsilon_r = 8.875$, $w/h = 1$, and $h = 0.508$ mm.). Present method (solid line) as compared to [2] (dashed line) and experiments (I) [2].

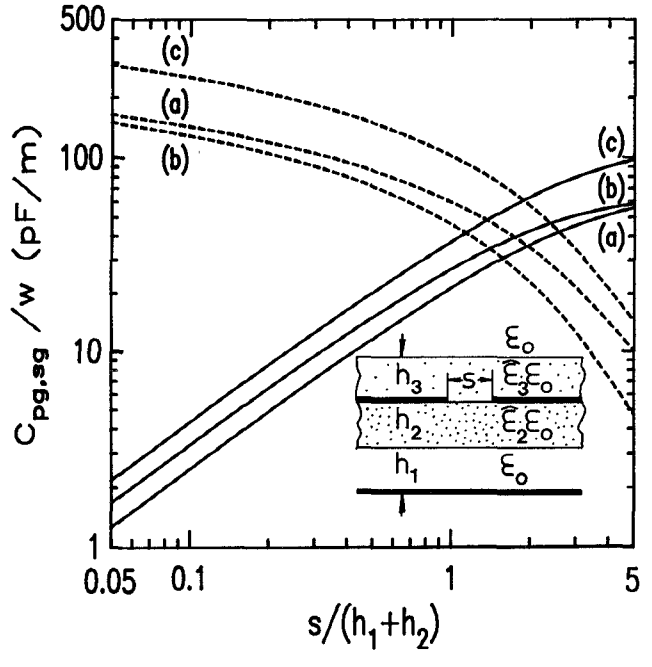

Fig. 7. Series and parallel capacitances of the equivalent circuit of a symmetric gap. Solid lines stand for C_{pg}/w. Dashed lines stand for C_{sg}/w. (a) Inverted configuration: (2) vacuum, (3) sapphire ($\epsilon_{11} = \epsilon_{33} = 9.4$, $\epsilon_{22} = 11.6$). (b) Suspended configuration: (3) vacuum, (2) sapphire ($\epsilon_{11} = \epsilon_{33} = 9.4$, $\epsilon_{22} = 11.6$). (c) Sandwiched configuration: (2) and (3) sapphire ($\epsilon_{11} = \epsilon_{33} = 9.4$, $\epsilon_{22} = 11.6$). In all cases, $h_1 = h_2 = h_3$ and $w/(h_1 + h_2) = 1$.

appearing in [8], in which the edge singularities have been very approximately included in the evaluation of the charge density existing on a rectangular patch. The average discrepancies with the results obtained in [6] and [9] lie around 5% and 20% respectively. In these two latter papers, the edge singularities have not been taken into account in the approximation of the excess charge density on an open-end strip and in the approximation of the charge density on a rectangular patch. We believe this omission produces the differences that have been found between those results and ours.

In Fig. 5, the edge capacitance per unit strip width of open-end discontinuities in sandwiched, suspended, and inverted configurations is plotted versus w/h. Comparison is made with the results reported in [7]. In this case, the discrepancies between our results and those reported in [7] lie between 5% and 15%.

In Fig. 6, we present results for the capacitances C_{sg} and C_{pg} of the equivalent circuit of a symmetric gap. The results are compared with those obtained by dynamic analysis and with measurements [2]. Our results seem to show a better agreement with experimental results than those obtained with dynamic analysis.

To show the versatility of the method of analysis described in this paper, in Fig. 7 we present original results for the capacitances C_{pg} and C_{sg} of the equivalent circuit of gap discontinuities printed on sapphire in sandwiched, suspended, and inverted configurations.

V. Conclusions

The lumped capacitances of the equivalent circuits which characterize the open-end and the symmetric gap microstrip discontinuities are calculated in an efficient and accurate way. These two discontinuities are considered to be embedded in a multilayered substrate involving uniaxial dielectric materials. The Galerkin method in the spectral domain is used to solve for the two-dimensional Fourier transform of the excess charge density existing on the strips of the discontinuities. The basis functions for approximating the excess charge density on the strips are chosen so as to fit the physical features of the problem as accurately as possible. The validity of the method is checked by testing its numerical convergence with respect to the number of basis functions and with respect to the distance from the end of the strips in which the excess charge is assumed to disappear. The results obtained are compared with those appearing in the literature and average discrepancies between 5% and 10% are observed. These discrepancies are attributed to the lack of accuracy of previously computed results. Original design graphs are presented in which the generality of the method of analysis built in this paper is demonstrated.

Appendix

In this appendix, we are going to explain the method employed to calculate the double integrals resulting in (9) for the case where the functions defined in (11) and (12)

are used to approximate $\sigma_{ex}(x,z)$. The rest of the double integrals that appear in the calculation of C_{oc}, C_{pg} and C_{sg} can be carried out in a similar way.

The integrals appearing in (9) have been split into two terms:

$$\Lambda^l_{nk} = \Omega^l_{nk} + \Lambda^l_{nk}|_{as} \tag{A1}$$
$$(n,k=0,\cdots,N_1;\ l=0,\cdots,N_2)$$

where

$$\Omega^l_{nk} = \int_{-\infty}^{+\infty}\int_{-\infty}^{+\infty}\left[\tilde{G}(\alpha,\beta)-\tilde{G}_{as}(\alpha,\beta)\right] \cdot\tilde{\sigma}^n_\infty(\alpha)\frac{1}{j\beta}\tilde{\sigma}^{k*}_\infty(\alpha)\tilde{\sigma}^{l*}(\beta)\,d\alpha\,d\beta \tag{A2}$$
$$(n,k=0,\cdots,N_1;\ l=0,\cdots,N_2)$$

and

$$\Lambda^l_{nk}|_{as} = \int_{-\infty}^{+\infty}\int_{-\infty}^{+\infty}\tilde{G}_{as}(\alpha,\beta)\tilde{\sigma}^n_\infty(\alpha)\frac{1}{j\beta}\tilde{\sigma}^{k*}_\infty(\alpha) \cdot\tilde{\sigma}^{l*}(\beta)\,d\alpha\,d\beta \tag{A3}$$

In (A3), $\tilde{G}_{as}(\alpha,\beta)$ stands for the asymptotic behavior of $\tilde{G}(\alpha,\beta)$, which can be expressed as

$$\tilde{G}_{as}(\alpha,\beta) = \frac{K}{\sqrt{\alpha^2+\beta^2}} \tag{A4}$$

where

$$K = \frac{1}{\sqrt{\epsilon^M_{11}\epsilon^M_{22}}+\sqrt{\epsilon^{M+1}_{11}\epsilon^{M+1}_{22}}}. \tag{A5}$$

To calculate the integrals appearing in (A2), we have first transformed the integration variables into polar coordinates, i.e.,

$$\Omega^l_{nk} = 4\int_0^{\pi/2}\int_0^{+\infty}\left[\tilde{G}(\gamma)-\tilde{G}_{as}(\gamma)\right] \cdot\tilde{\sigma}^n_\infty(\gamma,\theta)\frac{1}{j\gamma\sin\theta}\tilde{\sigma}^{k*}_\infty(\gamma,\theta)\tilde{\sigma}^{l*}(\gamma,\theta)\gamma\,d\gamma\,d\theta \tag{A6}$$
$$(n,k=0,\cdots,N_1;\ l=0,\cdots,N_2).$$

The integrals appearing in (A6) have been numerically computed. Since the integrands exponentially decay as $\gamma\to\infty$ (owing to the exponential decay of $\tilde{G}(\gamma)-\tilde{G}_{as}(\gamma)$), the infinite numerical integrals in the γ variable have been quickly performed.

The calculation of the integrals appearing in (A3) has been carried out in the spatial domain. By using Parseval's theorem, these integrals have been expressed as

$$\Lambda^l_{nk}|_{as} = 4\pi^2\int_0^{+\infty}\int_{-w/2}^{+w/2}\sigma^k_\infty(x)\sigma^l(z) \cdot\left[\int_{-\infty}^{\infty}\int_{-w/2}^{+w/2}G_{as}(x-x',z-z')\tfrac{1}{2}\,\mathrm{sg}(z') \cdot\sigma^n_\infty(x')\,dx'\,dz'\right]dx\,dz$$
$$(n,k=0,\cdots,N_1;\ l=0,\cdots,N_2) \tag{A7}$$

$\mathrm{sg}(z)$ being the sign function, and

$$G_{as}(x-x',z-z') = \frac{K}{\sqrt{(x-x')^2+(z-z')^2}} \tag{A8}$$

where K has been defined in (A5). When the functions defined in (12) and (13) are introduced into (A7), the integrals in the z and z' variables can be calculated in closed form. For the case of the pulse functions (see (12)), we obtain

$$\Lambda^l_{nk}|_{as} = 4\pi^2\int_{-w/2}^{+w/2}\int_{-w/2}^{+w/2}\left(\frac{4}{\pi^2w^2}\right)\frac{T_{2n}\left(\frac{2x'}{w}\right)}{\left[1-\left(\frac{2x'}{w}\right)^2\right]^{1/2}} \cdot\frac{T_{2k}\left(\frac{2x}{w}\right)}{\left[1-\left(\frac{2x}{w}\right)^2\right]^{1/2}}\mathscr{I}_l(x-x')\,dx\,dx'$$
$$(n,k=0,\cdots,N_1;\ l=0,\cdots,N_2). \tag{A9}$$

where $\mathscr{I}_l(x-x')$ can be written

$$\mathscr{I}_l(x-x') = \mathscr{P}_{l+1}(x-x') - \mathscr{P}_l(x-x') - \mathscr{Q}_{l+1}(x-x') + \mathscr{Q}_l(x-x') \tag{A10}$$
$$(l=0,\cdots,N_2)$$

and

$$\mathscr{P}_l(x-x') = \frac{K}{z_{l+1}-z_l}\left[z_l\ln\left(\sqrt{z_l^2+(x-x')^2}+z_l\right) -2\sqrt{z_l^2+(x-x')^2}\right]$$
$$(l=0,\cdots,N_2) \tag{A11}$$

$$\mathscr{Q}_l(x-x') = \frac{K}{z_{l+1}-z_l}\left[z_l\ln\left(\sqrt{z_l^2+(x-x')^2}-z_l\right)\right]$$
$$(l=0,\cdots,N_2). \tag{A12}$$

To compute the integrals appearing in (A9), we have consecutively applied Gauss–Chebyshev quadrature formulas, which account for the singularities of the integrand in the integration limits. Since numerical problems still appear owing to the logarithmic singularities of the integrands at $x=x'$ (see (A12)), the functions $\mathscr{Q}_l(x-x')$ appearing in (A12) have been rewritten

$$\mathscr{Q}_l(x-x') = \left[\mathscr{Q}_l(x-x') - 2\ln\left(\frac{|x-x'|}{\sqrt{2z_l}}\right)\right] + 2\ln\left(\frac{|x-x'|}{\sqrt{2z_l}}\right)$$
$$(l=0,\cdots,N_2). \tag{A13}$$

Since the terms enclosed between square brackets do not show any singularity when $x = x'$, they have been integrated by using Gauss–Chebyshev quadrature formulas. The singular logarithmic terms have been integrated in closed form by using [17, eq. (7)], and the orthogonality relations of Chebyshev polynomials.

References

[1] R. Jansen, "Hybrid mode analysis of end effects of planar microwave and millimeterwave transmission lines," *Proc. Inst. Elec. Eng.*, vol. 128., pt H, pp. 77–86, Apr. 1981.

[2] H.-Y. Yang, N. G. Alexopoulos, and D. R. Jackson, "Microstrip open-end and gap discontinuities in a substrate-superstrate structure," *IEEE Trans. Microwave Theory Tech.*, vol. 37, pp. 1542–1546, Oct. 1989.

[3] A. F. Thomson and A. Gopinath, "Calculation of microstrip discontinuity inductances," *IEEE Trans. Microwave Theory Tech.*, vol. MTT-23, pp. 648–655, Aug. 1975.

[4] A. Farrar and A. T. Adams, "Matrix methods for microstrip three-dimensional problems," *IEEE Trans. Microwave Theory Tech.*, vol. MTT-20, pp. 497–504, Aug. 1972.

[5] M. Maeda, "An analysis of gap in microstrip transmission lines," *IEEE Trans. Microwave Theory Tech.*, vol. MTT-20, pp. 390–396, June 1972.

[6] Y. Rahamat Samii, T. Itoh and R. Mittra, "A spectral domain analysis for solving microstrip discontinuity problems," *IEEE Trans. Microwave Theory Tech.*, vol. MTT-22, pp. 372–378, Apr. 1974.

[7] B. Bhat and S. K. Koul, "Lumped Capacitance, open-circuit end effects, and edge-capacitance of microstrip-like transmissions lines for microwave and millimeter-wave applications," *IEEE Trans. Microwave Theory Tech.*, vol. MTT-32, pp. 433–439, Apr. 1984.

[8] R. R. Boix and M. Horno, "Lumped capacitance and open-end effects of striplike structures in multilayered and anisotropic substrates," *IEEE Trans. Microwave Theory Tech.*, vol. 37, pp. 1523–1528, Oct. 1989.

[9] P. Silvester and P. Benedek, "Equivalent capacitance of microstrip open circuits," *IEEE Trans. Microwave Theory Tech.*, vol. MTT-20, pp. 511–516, Aug. 1972.

[10] P. Benedek and P. Silvester, "Equivalent capacitances for microstrip gaps and steps," *IEEE Trans. Microwave Theory Tech.*, vol. MTT-20, pp. 729–733, Nov. 1972.

[11] A. Gopinath and C. Gupta, "Capacitance parameters of discontinuities in microstrip lines," *IEEE Trans. Microwave Theory Tech.*, vol. MTT-26, pp. 831–836, Oct. 1978.

[12] M. Horno, F. L. Mesa, F. Medina, and R. Marqués, "Quasi-TEM analysis of multilayered, multiconductor, coplanar structures with dielectric and magnetic anisotropy including losses," *IEEE Trans. Microwave Theory Tech.*, vol. 38, pp. 1059–1068, Aug. 1990.

[13] S. Marchetti and T. Rozzi, "Electric field singularities in microwave integrated circuits (MIC)," in *Proc. 20th European Microwave Conf.*, Sept. 1990, pp. 823–828.

[14] D. W. Kammler, "Calculation of characteristic admittances and coupling coefficients for strip transmission line parameters," *IEEE Trans. Microwave Theory Tech.*, vol. MTT-16, pp. 925–937, Nov. 1968.

[15] A. E. Ruheli and P. A. Brennan, "Efficient capacitance calculations for three dimensional multiconductor systems," *IEEE Trans. Microwave Theory Tech.*, vol. MTT-21, pp. 76–82, Feb. 1973.

[16] J. Martel, "Analysis of integrated transmission lines discontinuities using the spectral technique" (in Spanish), M.Sc. thesis, University of Seville, Sept. 1990.

[17] G. M. L. Gladwell and S. Cohen, "A Chebyshev approximation method for microstrip problems," *IEEE Trans. Microwave Theory Tech.*, vol. MTT-23, pp. 865–870, Nov. 1975.

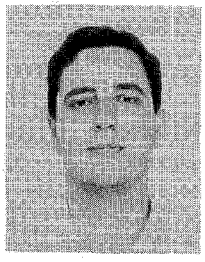

Jesús Martel was born in Seville, Spain, in December 1966. He received the B.Sc. (June 1989) and M.Sc. (October 1990) degrees in physics from the University of Seville, Spain. He is currently pursuing the Ph.D. degree there. His research interests are in the modeling of planar line discontinuities.

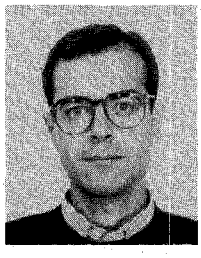

Rafael R. Boix was born in Melilla, Spain, in 1962. He received the B.Sc. (June 1985), the M.Sc. (September 1986), and the Ph.D. (October 1990) degrees in physics from the University of Seville, Spain.

Since 1990, he has been an Assistant Professor at the University of Seville, His research interests are in the modeling of planar line discontinuities and printed-circuit antennas.

Manuel Horno (M'75) was born in Torre del Campo, Jaén, Spain. He received the B.Sc. (June 1969) and Ph.D. degrees (January 1972) in physics from the University of Seville, Spain.

Since October 1969 he has been with the Department of Electricity and Electronics at the University of Seville, where he became an Assistant Professor in 1970, an Associate Professor in 1975, and Professor in 1986. His main fields of interest include boundary value problems in electromagnetic theory, wave propagation through anisotropic media, and microwave integrated circuits. He is presently engaged in the analysis of planar transmission lines embedded in anisotropic materials, multiconductor transmission lines, microstrip discontinuities, and planar slow-wave structures.